

# RSC Advances



This is an *Accepted Manuscript*, which has been through the Royal Society of Chemistry peer review process and has been accepted for publication.

*Accepted Manuscripts* are published online shortly after acceptance, before technical editing, formatting and proof reading. Using this free service, authors can make their results available to the community, in citable form, before we publish the edited article. This *Accepted Manuscript* will be replaced by the edited, formatted and paginated article as soon as this is available.

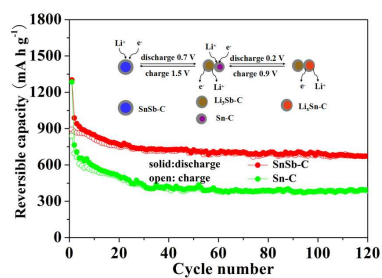
You can find more information about *Accepted Manuscripts* in the [Information for Authors](#).

Please note that technical editing may introduce minor changes to the text and/or graphics, which may alter content. The journal's standard [Terms & Conditions](#) and the [Ethical guidelines](#) still apply. In no event shall the Royal Society of Chemistry be held responsible for any errors or omissions in this *Accepted Manuscript* or any consequences arising from the use of any information it contains.

## Graphical Abstract

### Comparison between SnSb-C and Sn-C composites as anode materials for Li-ion batteries

Long Fan <sup>a</sup>, Jingjing Zhang <sup>a</sup>, Yongchun Zhu <sup>a, \*</sup>, Xiaobo Zhu <sup>a</sup>, Jianwen Liang <sup>a</sup>, Lili Wang <sup>a</sup>, and Yitai Qian <sup>a, b, \*</sup>



Benefiting from the synergistic effect of Sn and Sb, SnSb-C composite exhibited better electrochemical performances than that of Sn-C composite.

Cite this: DOI: 10.1039/c0xx00000x

www.rsc.org/xxxxxx

ARTICLE TYPE

## Comparison between SnSb-C and Sn-C composites as anode materials for lithium-ion batteries

Long Fan,<sup>a</sup> Jingjing Zhang,<sup>a</sup> Yongchun Zhu,<sup>\*a</sup> Xiaobo Zhu,<sup>a</sup> Jianwen Liang,<sup>a</sup> Lili Wang,<sup>a</sup> and Yitai Qian<sup>\*a,b</sup>

5 Received (in XXX, XXX) Xth XXXXXXXXXX 20XX, Accepted Xth XXXXXXXXXX 20XX

DOI: 10.1039/b000000x

SnSb-C and Sn-C composites have been fabricated by thermal annealing of the SnO<sub>2</sub>-Sb<sub>2</sub>O<sub>3</sub> and SnO<sub>2</sub> nanocomposite precursors under C<sub>2</sub>H<sub>2</sub>-pyrolysis reducing atmosphere, respectively. Both of the as-formed SnSb intermetallic compounds and Sn particles are uniformly dispersed in the synchronously formed continuous amorphous carbon matrix. As the anode for lithium-ion batteries, the SnSb-C composite shows a high reversible capacity of 672.2 mA h g<sup>-1</sup> after 120 cycles at a current density of 100 mA g<sup>-1</sup> together with a rate performance of 468.8 mA h g<sup>-1</sup> at 500 mA g<sup>-1</sup>, which are much better than those of the corresponding Sn-C composite (with similar carbon content as SnSb-C composite; 432.1 mA h g<sup>-1</sup> after 120 cycles at 100 mA g<sup>-1</sup> and 331.9 mA h g<sup>-1</sup> at 500 mA g<sup>-1</sup>). The better reversible capacity and cyclic performance of SnSb-C composite can be attributed to the synergistic effect and strong affinity between electrochemical Sn and Sb phases as well as the synchronously formed continuous amorphous carbon matrix.

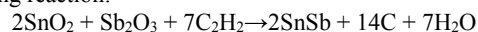
15

### 1. Introduction

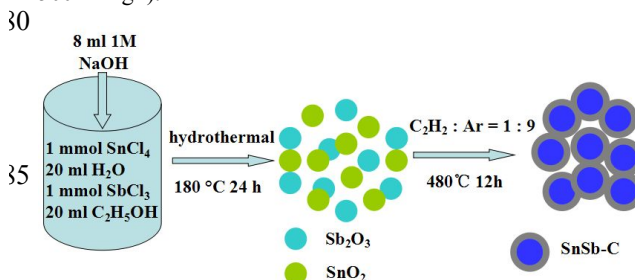
Rechargeable lithium-ion batteries (LIBs) based on commercial graphite anodes (theoretical capacity 372 mA h g<sup>-1</sup>) have attracted great interest as the power sources for various portable electronic devices.<sup>1-3</sup> The research of the electrode materials with higher capacity is one of the most widely investigated topics in LIBs. As previously reported, Sn-based anode materials have attracted much attention due to their high theoretical capacity (990 mA h g<sup>-1</sup>).<sup>4-8</sup> Nevertheless, the serious volume change during the Li<sup>+</sup> insertion and extraction process leads to rapid deterioration of cycling performance, which greatly delays their commercial implementation.<sup>5-7, 9-11</sup> To overcome the problem, one promising approach is incorporating of electrochemically active/inactive elements into tin to prepare intermetallic compounds (Sn-M), such as Cu<sub>6</sub>Sn<sub>5</sub>,<sup>12</sup> CoSn<sub>3</sub>,<sup>13-14</sup> FeSn<sub>2</sub>,<sup>15-16</sup> SnSb,<sup>17-24</sup> Ni<sub>3</sub>Sn<sub>4</sub> etc.<sup>25</sup> It has been reported that the cycling performance of Sn-M materials are significantly improved as the extruded M are expected as a buffer matrix to alleviate the expansion of tin based particles during the electrochemical cycling.<sup>16, 24</sup> What is more, carbon matrix supporting is regard as another promising method to improve the electrochemical performance as carbon is conductive and flexible to accommodate the strain of volume changes during Li<sup>+</sup> insertion/extraction process.<sup>23, 26-30</sup> Among various Sn-M anodes, all active SnSb intermetallic compounds (or SnSb-C composite) have been considered promising.<sup>31-39</sup> Firstly, both Sn (990 mA h g<sup>-1</sup>) and Sb (660 mA h g<sup>-1</sup>) are electrochemical active, which contribute to the overall specific capacity. Secondly, as the lithium insertion/extraction reactions of Sn and Sb occur at different potentials, the unreacted phases can serve as a buffer matrix to accommodate volume change yielded by the reacted phases, thus reducing the mechanical strain and improving the structural stability of the whole electrode.<sup>11, 24, 35</sup> In addition, Sb displays higher Li intercalation potential than that of Sn phase in discharge process and the SnSb intermetallic compounds can be reversed back to original phase after lithium extraction process.<sup>18, 41</sup> According to

the previous reports, by mixing the as-spun SnSb nanocrystalline with the acid treated carbon nanotubes, the obtained SnSb-carbon nanotube network nanocomposites shows lithium storage capacity of 860 mA h g<sup>-1</sup> at a current of 160 mA g<sup>-1</sup> after 40 cycles.<sup>35</sup> Porous SnSb-C nanocomposite displays a reversible capacity of 420 mA h g<sup>-1</sup> at a current of 100 mA g<sup>-1</sup> after 50 cycles.<sup>33</sup>

In this study, a SnSb-C composite is prepared by thermal annealing of SnO<sub>2</sub>-Sb<sub>2</sub>O<sub>3</sub> nanocomposite precursor under C<sub>2</sub>H<sub>2</sub>-pyrolysis reducing atmosphere, in which the SnSb particles with size about 300 nm are uniformly dispersed in the synchronously formed amorphous carbon matrix. The C<sub>2</sub>H<sub>2</sub> adopted in the preparing process is not only as the carbon precursor, but also as the reductive agent which promotes the reduction of Sn<sup>4+</sup> and Sb<sup>3+</sup> to form SnSb. This process can be described as the following reaction:



With the synergistic effect and strong affinity between Sn and Sb phases and the synchronously formed continuous supporting carbon matrix, the SnSb-C composite demonstrates a high reversible capacity (672.2 mA h g<sup>-1</sup> after 120 cycles at 100 mA g<sup>-1</sup>) and good rate performance (468.8 mA h g<sup>-1</sup> at 500 mA g<sup>-1</sup>), which are much better than those of the Sn-C composite (432.1 mA h g<sup>-1</sup> after 120 cycles at 100 mA g<sup>-1</sup> and 331.9 mA h g<sup>-1</sup> at 500 mA g<sup>-1</sup>).



**Scheme 1** Illustration of the formation process for SnSb-C composite.

## 2. Experimental

### 2.1. Preparation of SnO<sub>2</sub>-Sb<sub>2</sub>O<sub>3</sub> and SnO<sub>2</sub> nanocomposite precursors

SnO<sub>2</sub>-Sb<sub>2</sub>O<sub>3</sub> nanocomposite was prepared by a co-precipitation approach. All chemicals were of analytical grade and used without further purification. In a typical synthesis, 1 mmol SbCl<sub>3</sub> and 1 mmol SnCl<sub>4</sub>·5H<sub>2</sub>O were added to a 40 mL mixture solution of ethanol and water (1/1; v/v) under magnetic stirring. When the mixture was dispersed to form a homogeneous solution, 8 mL 1 M NaOH solution was dropwise added to the above solution at ambient temperature under magnetic stirring and a white mixture was formed. After stirred for 1 h, the solution was transferred into a Teflon-lined autoclave with a capacity of 60 mL. The autoclave was sealed and maintained at 180 °C for 24 h. After cooled to ambient temperature, the resulting product was collected and washed with deionized water and ethanol for several times and then dried under vacuum at 50 °C for 12 h. The product was prepared for further process and characterization. Meanwhile, the SnO<sub>2</sub> nanoparticles were prepared via the similar approach without adding SbCl<sub>3</sub>.

### 2.2. Preparation of SnSb-C and Sn-C composites

SnSb-C composite was prepared by thermal annealing C<sub>2</sub>H<sub>2</sub> with the precursor of SnO<sub>2</sub>-Sb<sub>2</sub>O<sub>3</sub> nanocomposite as our previous work.<sup>30</sup> Typically, the dried SnO<sub>2</sub>-Sb<sub>2</sub>O<sub>3</sub> nanocomposite precursors were annealed in a furnace at 480 °C under continuous C<sub>2</sub>H<sub>2</sub>/argon gas flow (1/9; v/v) for 12 h with the heating rate of 3 °C min<sup>-1</sup>. After naturally cooled to room temperature, the black powder was collected for later characterization. The Sn-C composite was prepared by annealed SnO<sub>2</sub> nanoparticles precursor at 420 °C under continuous C<sub>2</sub>H<sub>2</sub>/argon gas flow (1/9; v/v) for 12 h via the similar protocol.

### 2.3. Material characterization

The as-prepared composites were characterized by powder X-ray diffraction (XRD) using a Philips X'pert X-ray diffractometer with Cu Kα radiation (λ=1.541874 Å). Raman spectra were taken by using a JYLABRAM-HR Confocal Laser Micro-Raman spectrometer. Carbon content was measured on a vario EL-III elemental analyzer. Inductively coupled plasma (ICP) atomic emission spectrometer (PerkinElmer Instruments) was used to measure the ratio of metal atoms. The morphologies were investigated by using a field-emitting scanning electron microscope (SEM, JEOL-JSM-6700F) and transmission electron microscope (TEM, H7650). HRTEM images and the elements distribution and EDS profile were probed by energy-dispersive X-ray spectrometry (EDX) elemental mapping analysis (JEM-ARM 200F).

### 2.4. Electrochemical measurements

The electrochemical performance versus Li was tested by using coin-type 2016 cells. The working electrodes for electrochemical testing consisted of the active materials, super P carbon black,

and polyvinylidene fluoride (PVDF) with a weight ratio of 70 : 50 : 20 : 10. The loading of active material in the electrode was about 2.16 mg cm<sup>-2</sup>. The coin cells were assembled in an argon-filled glove box (Celgard 2400) with Li metal as an anode and the solution of 1 mol L<sup>-1</sup> LiPF<sub>6</sub> in ethylene carbonate (EC)/diethyl carbonate (DEC) (1/1; v/v) as the electrolyte. Cyclic voltammograms (CV) were measured by CHI650A electrochemical workstation. The galvanostatic discharge/charge tests were performed on a battery cycler (Land-CT2001A) with the voltage range of 0.01-2.50 V (vs. Li/Li<sup>+</sup>) at different current densities. The EIS were performed on CHI660D electrochemical workstation.

## 3. Results and Discussion

The formation process of SnSb-C composite is illustrated in Scheme 1. Firstly, SnO<sub>2</sub>-Sb<sub>2</sub>O<sub>3</sub> nanocomposite precursor is hydrothermally synthesized via a metathesis reaction (2SnCl<sub>4</sub> + 2SbCl<sub>3</sub> + 14NaOH → 2SnO<sub>2</sub> + Sb<sub>2</sub>O<sub>3</sub> + 14NaCl + 7H<sub>2</sub>O). After removing the byproduct of NaCl, the SnO<sub>2</sub>-Sb<sub>2</sub>O<sub>3</sub> nanocomposite precursor is further treated by thermal reduction deposition of C<sub>2</sub>H<sub>2</sub>/argon gas flow to prepare the SnSb-C composite. The formation reaction can be described as equation (1) in the introduction and the final product is obtained. The Sn-C composite is prepared via the similar approach.

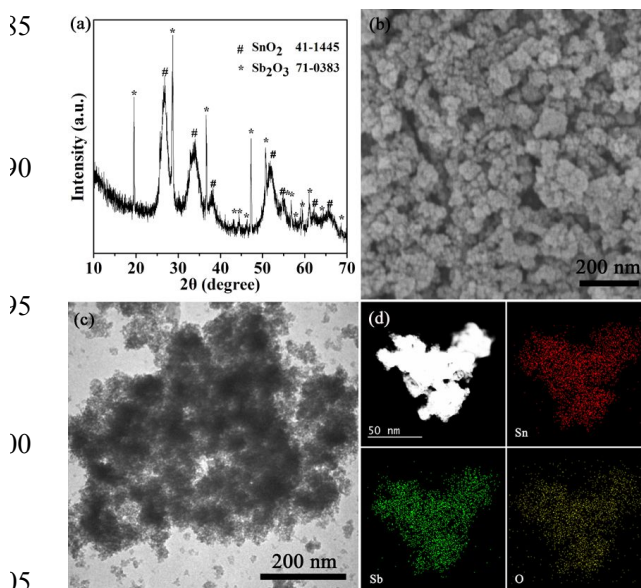


**Figure 1** (a) XRD pattern, (b) SEM image (c) TEM image of the SnO<sub>2</sub>-Sb<sub>2</sub>O<sub>3</sub> nanocomposite precursor (d) The bright-field STEM image and the EDX maps of Sn, Sb, and O, respectively.

### SnO<sub>2</sub>-Sb<sub>2</sub>O<sub>3</sub> and SnO<sub>2</sub> precursors characterization.

The crystallographic structure and phase purity of the SnO<sub>2</sub>-Sb<sub>2</sub>O<sub>3</sub> precursor is examined by XRD, as shown in Figure 1a. The diffraction peaks demonstrate two phases which are consistent with the tetragonal phase of cassiterite SnO<sub>2</sub> (JCPDS card No. 41-1445) and the orthorhombic antimonous oxide Sb<sub>2</sub>O<sub>3</sub> (JCPDS card No. 71-0383). ICP analysis demonstrates the atomic ratio of Sn and Sb is about 1.04 : 1. The size and morphology of the as obtained SnO<sub>2</sub>-Sb<sub>2</sub>O<sub>3</sub> precursor are investigated by SEM (Figure 1b) and TEM (Figure 1c). The SEM image shows that the

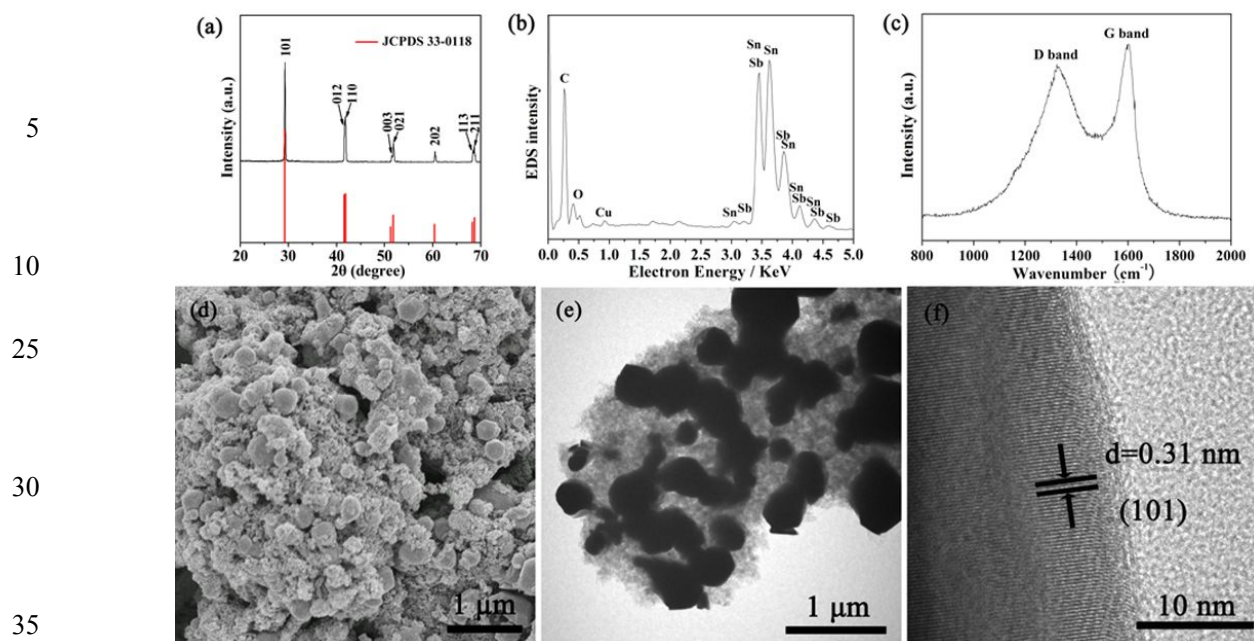


**Figure 2** (a) XRD pattern, (b) EDS profile, (c) Raman spectrum, (d) SEM image, (e) TEM image and (f) HRTEM image of SnSb-C composite.

precursor is consisted of nanoparticles with particle size of 40 nm. Further TEM image demonstrates that these nanoparticles are composed of much smaller nanoparticles with the sizes about 5 nm. The EDX mappings (Figure 1d) reveal the Sn and Sb elements are uniformly dispersed in the SnO<sub>2</sub>-Sb<sub>2</sub>O<sub>3</sub> precursor. The SEM and TEM images (Figure S1) show that the SnO<sub>2</sub> nanoparticles are consist of nanoparticles with the size of about 5 nm.

### 50 SnSb-C and Sn-C composites characterization.

The phase purity of the as-prepared SnSb-C sample is examined by XRD. All the reflection peaks in Figure 2a can be indexed as rhombohedral β-SnSb phase (JCPDS card No 33-0118). The sharp observed peaks confirm the good crystallinity of SnSb intermetallic compounds. A typical EDS spectrum of the SnSb-C composite is shown in Figure 2b. The quantitative analysis of the spectrum demonstrates that the mole ratio of Sn and Sb in the SnSb-C composite is about 1.05 : 1, which is consistent with the ICP analysis result (1.04 : 1). Figure 2c shows that there are two peaks locating at about 1345 and 1610 cm<sup>-1</sup>, corresponding to the characteristic D-band (the disordered band) and G-band (the graphene band) of graphite carbon, which suggests the presence of carbon in the sample. While, the I<sub>D</sub>/I<sub>G</sub> ratio of the product is calculated to be 0.91, indicating the carbon is fairly amorphous.<sup>42</sup> Besides, the carbon content in SnSb-C composite can be readily determined by vario EL-III elemental analysis to be about 20.82 wt%. Figure 2d shows the SEM image of SnSb-C composite, which clearly indicates the SnSb particles with an average size of 300 nm are supported by carbon matrix. Compared with the original SnO<sub>2</sub>-Sb<sub>2</sub>O<sub>3</sub> nanocomposite precursor, the particles after annealed process have much bigger sizes. TEM image in Figure 2e indicates the supporting carbon matrix with a continued structure is tightly attached to the SnSb particles, which could facilitate mechanical reinforcement and enhance electronic conductivity. The HRTEM image (Figure 2f) displays lattice

fringes of 0.31 nm, in accordance with the (101) lattice planes of β-SnSb. Figure S2 shows the SEM image of Sn-C composite, which clearly indicates the consistent of nanoparticles and short nanorods. It is worth noting that these short nanorods are may assembled from small nanoparticles during the sintered process. Further TEM observation demonstrates the carbon matrix supported Sn component by showing notable contrast difference between the pale matrix and the dark center. Besides, the carbon content in the Sn-C sample, carries out by element analysis on a vario EL-III elemental analyzer, is approximately 21.58 wt%.

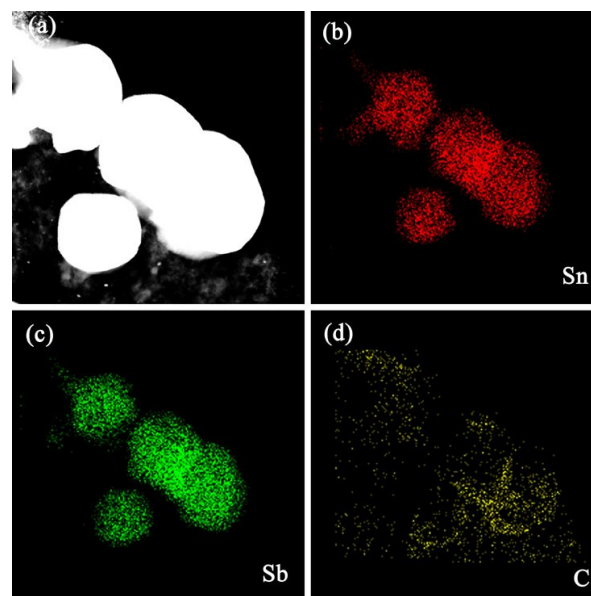


**Figure 3** (a) The bright-field STEM image of the SnSb-C composite; (b-d) EDX maps of Sn, Sb, and C, respectively.

In order to obtain the element distribution in the SnSb-C composite, a bright-field STEM image and the corresponding EDX elemental maps are conducted, as shown in Figure 3a-3d. It can be concluded from comparing the Sn and Sb map images that these two elements are uniformly dispersed in the SnSb-C composite. The carbon map (Figure 3d) shows the location of carbon deposits on the whole SnSb particles, which indicates the SnSb particles are uniformly dispersed in the synchronously formed continuous amorphous carbon matrix.

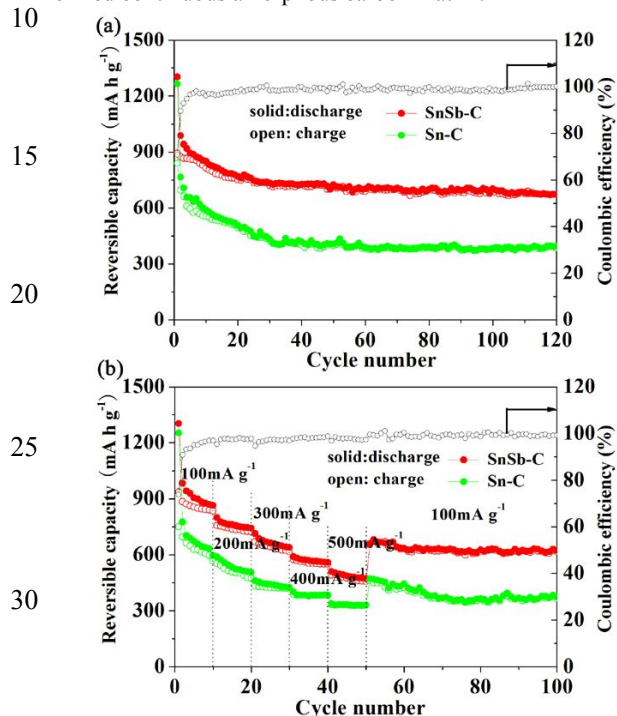


**Figure 4** (a) cycling performance at a current density of 100 mA g<sup>-1</sup> from 0.01 to 2.5 V and (b) rate performance at various current densities for the SnSb-C and Sn-C composites.

#### SnSb-C and Sn-C composites electrochemical performance.

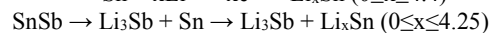
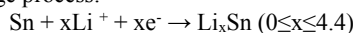
The electrochemical behaviors of the SnSb-C and Sn-C composites are investigated as anode materials for LIBs and the specific capacities are calculated on the whole mass of the composite (SnSb + C or Sn + C). Figure 4a shows the cycling performance of SnSb-C and Sn-C composite with a voltage window from 0.01 V to 2.5 V at a current density of 100 mA g<sup>-1</sup>. The first discharge and charge capacities of the SnSb-C composite are 1302.2 and 914.9 mA h g<sup>-1</sup>, respectively, corresponding to a coulombic efficiency of 71%. The capacity loss in the first cycle (387.3 mA h g<sup>-1</sup>) is mainly attributed to the initial irreversible formation of a solid electrolyte interphase (SEI) layer and other irreversible processes.<sup>23, 33, 35</sup> Nevertheless, from the second cycle onward, the coulombic efficiency is gradually rising to 100% and the SnSb-C composite retains a stable capacity of approximately 672.2 mA h g<sup>-1</sup> after 120 cycles. In comparison with the recent reports on various SnSb-C anode materials, the SnSb-C (this work) also shows high reversible capacity and excellent cycle stability (Table. S1). Conversely, the Sn-C composite electrode delivers a reversible capacity of about 839.4 mA h g<sup>-1</sup> in the initial cycle with a coulombic efficiency of 65%. However, its specific capacity is gradually dropping to around 432.2 mA h g<sup>-1</sup> after 30 cycles and maintaining this

reversible capacity after the following 90 cycles, which is much lower than that of SnSb-C composite.

The rate performances of two composites are further illustrated in Figure 4b. As the current density increasing from 100 to 200, 300, 400 and 500 mA g<sup>-1</sup>, the average reversible capacities of SnSb-C composite are 898.7, 755.8, 662.1, 566.1 and 468.8 mA h g<sup>-1</sup>, respectively. Upon altering the current density back to 100 mA g<sup>-1</sup>, the reversible capacity can be recovered to 633.1 mA h g<sup>-1</sup> during the following 50 cycles. While, in the same current densities, the reversible capacities of Sn-C composite are 672.7, 521.7, 440.9, 381.7 and 331.9 mA h g<sup>-1</sup>, respectively, and the following reversible capacity is keeping around 423.5 mA h g<sup>-1</sup>.

Apparently, the SnSb-C composite demonstrates better cyclic capacity retention and rate performance than those of Sn-C composite (with similar carbon content as SnSb-C composite). To better understand the physical/chemical behavior of the SnSb-C composite during electrochemical cycles, further studies are carried out. Figure 5a and 5b compare the CVs of the SnSb-C and Sn-C composite for the initial three cycles at a scan rate of 0.1 mV s<sup>-1</sup> in the voltage range of 0.01-2.5 V v.s. Li/Li<sup>+</sup>. Four intense oxidation peaks range from 0.55 to 0.89 V and reduction peaks around 0.3 V are assigned to the multi-step delithiation and lithiation reaction of the Li<sub>x</sub>Sn alloy, which can be observed in both SnSb-C and Sn-C composite electrode.<sup>11, 24, 35, 41 43-44</sup> However, a couple of cathodic/anodic peaks locating around 0.71 and 1.17 V (Figure 5a), corresponding to the reactions between Sb and Li, are only exist in SnSb-C composite electrode.<sup>33, 35-38</sup> Both of the lithiation and delithiation voltages of Sb (0.71 and 1.17 V, respectively) are higher than those of Sn, which indicates the electrochemical cycles of SnSb-C composite electrode with a stepwise manner and makes the volume changes much smoothly.<sup>11, 35, 39</sup> Therefore, the general electrochemical reactions of Sn-C and SnSb-C composite electrode can be summarized as the previous studies:<sup>4-5, 39-41, 43-44</sup>

Discharge process:



Charge process:

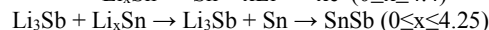
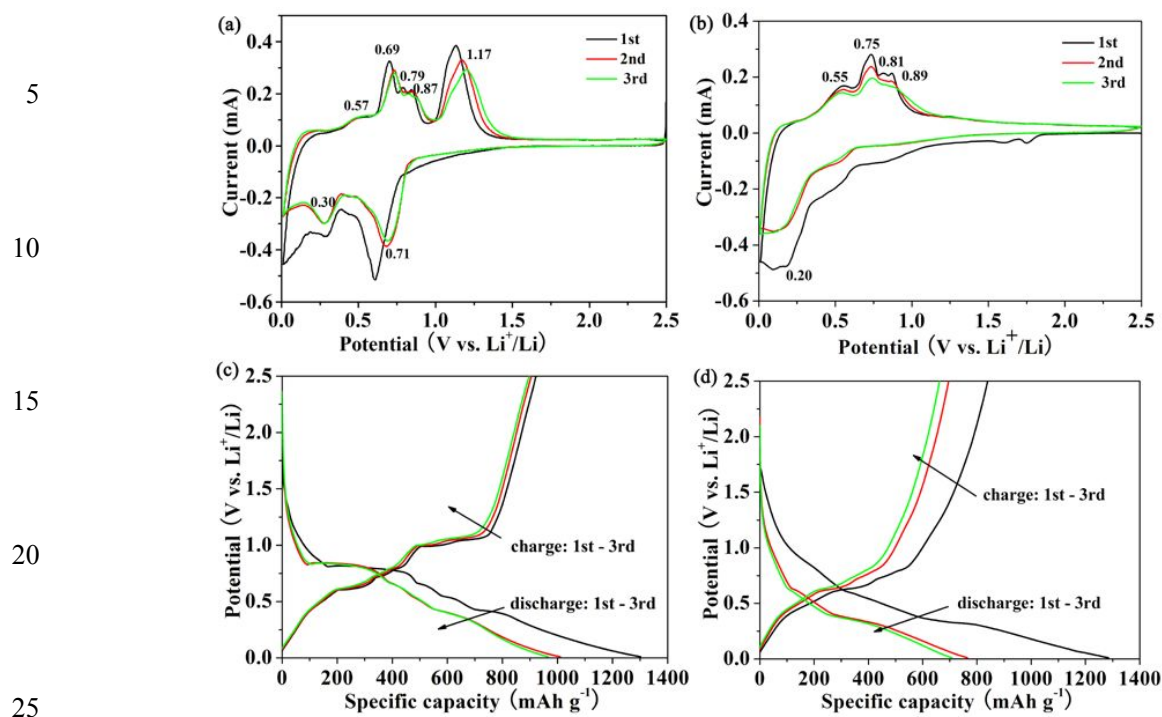
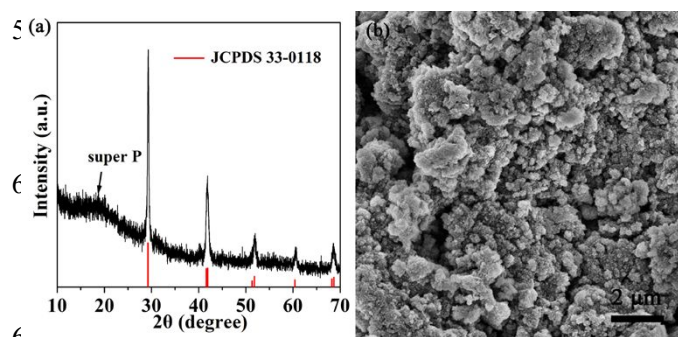


Figure 5c-5d show the discharge/charge voltage profiles of the SnSb-C and Sn-C composites electrode with cutoff voltage range of 0.01-2.5 V for the initial three cycles at 100 mA g<sup>-1</sup>. The voltage plateaus around 0.8 V (discharge curve) and 1.1 V (charge curve) can be only observed in SnSb-C composite electrode, which are consistent well with the CV results.

Figure 6a shows the XRD pattern of SnSb-C composite after 5 cycles at 100 mA g<sup>-1</sup>. It can be seen that the crystal structure of β-SnSb is restored after 5 cycles, which implies that the Sn and Sb atoms have a strong affinity with each other and the structure of β-SnSb phase is stable.<sup>18</sup> Such self-restoration is favorable for the electrochemical performance of the SnSb anode.<sup>18, 39, 41</sup> The morphology and EDX elemental mapping of SnSb-C composite after 120 charge/discharge cycles at 100 mA g<sup>-1</sup> are presented in Figure 6b and Figure 3S. The sample almost maintains its morphology of particles uniformly dispersing in carbon matrix and element Sn and Sb are uniformly distributed.



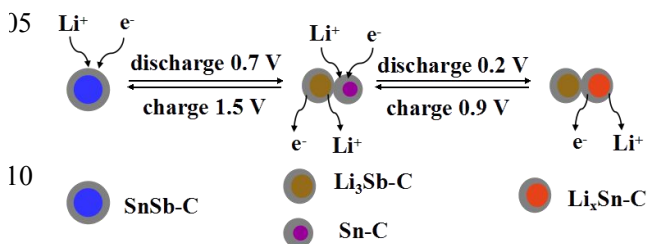
**Figure 5** CV of the initial 3th cycles scanned between 0.01-2.5 V v.s.  $\text{Li}/\text{Li}^+$  at a rate of  $0.1 \text{ mV s}^{-1}$ : (a) SnSb-C composite, (b) Sn-C composite; Discharge/charge voltage profiles at  $100 \text{ mA g}^{-1}$ : (c) SnSb-C composite, (d) Sn-C composite.



**Figure 6** (a) XRD pattern of SnSb-C composite after 5 charge/discharge cycles at  $100 \text{ mA g}^{-1}$ , (b) SEM image of SnSb-C composite after 120 charge/discharge cycles at  $100 \text{ mA g}^{-1}$ .

Scheme 2 illustrates the possible mechanism of the interactional buffer effect in the SnSb-C composite during the electrochemical cycles. Combined with the previous reports and CV curves (Figure 5a), the SnSb-C composite involves two electrochemical reactions.<sup>11, 18, 23, 39, 41</sup> At the stage of discharge, the lithiation reaction of Sb takes place firstly to produce  $\text{Li}_3\text{Sb}$  phase at a higher potential (e.g.  $0.71 \text{ V}$ ), while the ductile Sn phase is hardly to alloy with Li so as to serves as electrical connections for the Sb phase.<sup>11, 39, 41</sup> When the discharge continues to a low potential region (e.g.  $0.4 \text{ V}$ ), Sn phase alloys with Li to form various  $\text{Li}_x\text{Sn}$  alloys and the as formed  $\text{Li}_3\text{Sb}$  phase can act as a buffer framework to accommodate the volume expansion of  $\text{Li}_x\text{Sn}$  phase. During reversed charge, the  $\text{Li}_x\text{Sn}$  phase and  $\text{Li}_3\text{Sb}$  phase recover back to original SnSb phase separately.<sup>18</sup> Benefiting from this synergistic effect between the

Sb and Sn phases, the volumetric changes are alleviated in the lithiation/delithiation process, which improves the cycling stability of SnSb-C composite. Moreover, the synchronously formed continuous amorphous carbon matrix also plays an important role to the excellent electrochemical performance of SnSb-C composite, as it not only provides good electronic conductivity and  $\text{Li}^+$  mobility property but also acts as a supporting matrix to make the synchronously formed SnSb particles uniformly dispersing in the sample, thus accommodating the volume changes and structural stress.<sup>23, 30-33</sup> The superior electronic conductivity of SnSb-C was confirmed by the obviously reduced diameter of the semicircle at the high-to-medium frequency region in the electrochemical impedance spectroscopy (EIS) patterns (Figure S4). Such synergistic approaches in the SnSb-C composite could be promising for the development of other multi-elements composite anode materials for LIBs.



**Scheme 2** Illustration of the possible lithiation and delithiation process of SnSb-C composite.

## 4. Conclusions

In summary, we have synthesized SnSb-C and Sn-C composites via thermal annealing of the SnO<sub>2</sub>-Sb<sub>2</sub>O<sub>3</sub> and SnO<sub>2</sub> nanocomposite precursors under C<sub>2</sub>H<sub>2</sub>-pyrolysis reducing atmosphere. The prepared SnSb-C composite exhibits enhanced cyclability and rate performance than those of Sn-C composite (with similar carbon content as SnSb-C composite). The excellent electrochemical performance of SnSb-C composite are mainly attributed to: (1) the synergistic effect and strong affinity between Sn and Sb phases, which leads the SnSb-C composite electrode undergoing with a stepwise manner and making the volume changes much smoothly; (2) the synchronously formed continuous amorphous carbon matrix, which enables the synchronously formed SnSb particles uniformly dispersing in the sample, thereby accommodating the volume changes and structural stress of the whole electrode. Such synthesis approaches and synergetic strategies in the SnSb-C composite may supply a new way to explore other advanced intermetallic compounds electrode for LIBs.

## Acknowledgements

This work was supported by the National Natural Science Fund of China (No. 91022033, 21201158), the 973 Project of China (No. 2011CB935901).

## Notes and references

<sup>a</sup> Hefei National Laboratory for Physical Science at Microscale and Department of Chemistry, University of Science and Technology of China, Hefei, 230026, P.R. China. Tel: +86-551-63601589; E-mail: ychzhu@ustc.edu.cn

<sup>b</sup> School of Chemistry and Chemical Engineering, Shandong University, Jinan, 250100, PR China. Tel: +86-551-63607234; E-mail: ytqian@ustc.edu.cn

\*Corresponding author: ychzhu@ustc.edu.cn (Y. C. Zhu) ytqian@ustc.edu.cn (Y. T. Qian)

† Electronic Supplementary Information (ESI) available. See DOI: 10.1039/b000000x/

- 1 M. Armand, J. M. Tarascon, *Nature*, 2008, **451**, 652-657.
- 2 M. Winter, J. O. Besenhard, M. Spahr, P. Novak, *Adv. Mater.*, 1998, **10**, 725-763.
- 3 Y. M. Chen, Z. G. Lu, L. M. Zhou, Y. W. Mai, H. T. Huang, *Energy Environ. Sci.*, 2012, **5**, 7898-7902.
- 4 R. A. Huggins, *J. Power Sources*, 1999, **81-82**, 13-19.
- 5 M. Winter, J. O. Besenhard, *Electrochim. Acta*, 1999, **45**, 31-50.
- 6 W. J. Zhang, *J. Power Sources*, 2011, **196**, 13-24.
- 7 C. M. Park, J. H. Kim, H. Kim, H. J. Sohn, *Chem. Soc. Rev.*, 2010, **39**, 3115-3141.
- 8 J. S. Chen, X. W. Lou, *small*, 2013, **9**, 1877-1893.
- 9 J. Y. Huang, L. Zhong, C. M. Wang, J. P. Sullivan, W. Xu, L. Q. Zhang, S. X. Mao, N. S. Hudak, X. H. Liu, A. Subramanian, H. Y. Fan, L. Qi, A. Kushima, J. Li, *Science*, 2010, **330**, 1515-1520.
- 10 L. P. Xu, C. J. Kim, A. K. Shukla, A. Dong, T. M. Mattox, D. J. Milliron, J. Cabana, *Nano Lett.*, 2013, **13**, 1800-1805.
- 11 S. C. Chao, Y. F. Song, C. C. Wang, H. S. Sheu, H. C. Wu, N. L. Wu, *J. Phys. Chem. C*, 2011, **115**, 22040-22047.
- 12 W. J. Cui, F. Wang, J. Wang, H. J. Liu, C. X. Wang, Y. Y. Xia, *J. Power Sources*, 2011, **196**, 3633-3639.
- 13 C. X. Zhai, N. Du, H. Zhang, J. X. Yu, P. Wu, C. M. Xiao, D. R. Yang, *Nanoscale*, 2011, **3**, 1798-1801.
- 14 Y. Gu, F. D. Wu, Y. Wang, *Adv. Funct. Mater.*, 2013, **23**, 893-899.
- 15 M. Chamas, P. E. Lippens, J. C. Jumasa, K. Boukerma, R. Dedryvère, D. Gonbeau, J. Hassoun, S. Panero, B. Scrosati, *J. Power Sources*, 2011, **196**, 7011-7015.
- 16 X. L. Wang, M. Feyngenson, H. Y. Chen, C. H. Lin, W. Ku, J. M. Bai, M. C. Aronson, T. A. Tyson, W. Q. Han, *J. Am. Chem. Soc.*, 2011, **133**, 11213-11219.
- 17 J. Yang, M. Winter, J. O. Besenhard, *Solid State Ionics*, 1996, **90**, 281-287.
- 18 H. Li, G. Y. Zhu, X. J. Huang, L. Q. Chen, *J. Mater. Chem.*, 2000, **10**, 693-696.
- 19 J. O. Besenhard, J. Yang, M. Winter, *J. Power Sources* 1997, **68**, 87-90.
- 20 J. Yang, Y. Takeda, N. Imanishi, O. Yamamoto, *J. Electrochem. Soc.* 1999, **146**, 4009-4013.
- 21 M. Wachtler, M. Winter, J. O. Besenhard, *J. Power Sources* 2002, **105**, 151-160.
- 22 H. Li, Q. Wang, L. H. Shi, L. Q. Chen, X. J. Huang, *Chem. Mater.*, 2002, **14**, 103-108.
- 23 M. S. Park, S. A. Needham, G. X. Wang, Y. M. Kang, J. S. Park, S. X. Dou, H. K. Liu, *Chem. Mater.*, 2007, **19**, 2406-2410.
- 24 H. L. Zhao, C. L. Yin, H. Guo, J. C. He, W. H. Qiu, Y. Li, *J. Power Sources*, 2007, **174**, 916-920.
- 25 K. K. D. Ehinon, S. Naille, R. Dedryvère, P. E. Lippens, J. C. Jumas, D. Gonbeau, *Chem. Mater.*, 2008, **20**, 5388-5398.
- 26 H. Q. Li, H. S. Zhou, *Chem. Commun.*, 2012, **48**, 1201-1217.
- 27 G. Derrien, J. Hassoun, S. Panero, B. Scrosati, *Adv. Mater.*, 2007, **19**, 2336-2340.
- 28 Z. Y. Wang, Z. C. Wang, W. T. Liu, W. Xiao, X. W. Lou, *Energy Environ. Sci.*, 2013, **6**, 87-91.
- 29 L. Zhang, G. Q. Zhang, H. B. Wu, L. Yu, X. W. Lou, *Adv. Mater.*, 2013, **25**, 2589-2593.
- 30 L. Fan, Y. C. Zhu, J. J. Zhang, J. W. Liang, L. L. Wang, D. H. Wei, X. N. Li, Y. T. Qian, *Electrochim. Acta*, 2014, **121**, 21-26.
- 31 J. Hassoun, G. Derrien, S. Panero, B. Scrosati, *Electrochim. Acta*, 2009, **54**, 4441-4444.
- 32 S. Q. Chen, P. Chen, M. H. Wu, D. Y. Pan, Y. Wang, *Electrochem. Commun.*, 2010, **12**, 1302-1306.
- 33 C. M. Park, K. J. Jeon, *Chem. Commun.* 2011, **47**, 2122-2124.
- 34 F. S. Ke, L. Huang, B. C. Solomon, G. Z. Wei, L. J. Xue, B. Zhang, J. T. Li, X. D. Zhou, S. G. Sun, *J. Mater. Chem.*, 2012, **22**, 17511-17517.
- 35 S. F. Fan, T. Sun, X. H. Rui, Q. Y. Yan, H. H. Hng, *J. Power Sources*, 2012, **201**, 288-293.
- 36 J. Li, Q. Ru, S. J. Hu, D. W. Sun, B. B. Zhang, X. H. Hou, *Electrochim. Acta*, 2013, **113**, 505-513.
- 37 L. G. Xue, X. Xia, T. Tucker, K. Fu, S. Zhang, S. L. Li, X. W. Zhang, *J. Mater. Chem. A*, 2013, **1**, 13807-13813.
- 38 J. Y. Zhang, Z. Y. Wang, Y. Z. Hong, S. X. Li, X. B. Jin, G. Z. Chen, *Electrochem. Commun.*, 2014, **38**, 36-39.
- 39 C. M. Park, H. J. Sohn, *Electrochim. Acta* 2009, **54**, 6367-6373.
- 40 F. J. Fernández-madrugalet, P. Lavela, C. P. Vicente, J. L. Tirado, *Chem. Mater.* 2002, **14**, 2962-2968.
- 41 J. U. Seo, C. M. Park, *J. Mater. Chem. A* 2013, **1**, 15316-15322.
- 42 A. C. Ferrari, J. Robertson, *Phys. Rev. B*, 2000, **61**, 14095-14107.
- 43 Z. Tan, Z. H. Sun, H. H. Wang, Q. Guo, D. S. Su, *J. Mater. Chem. A*, 2013, **1**, 9462-9468.
- 44 Y. H. Xu, Q. Liu, Y. J. Zhu, Y. H. Liu, A. Langrock, M. R. Zachariah, C. S. Wang, *Nano Lett.*, 2013, **13**, 470-474.